
Simultaneous Similarity-based Self-Distillation for Deep Metric Learning

Karsten Roth^{1,2} Timo Milbich² Björn Ommer² Joseph Paul Cohen^{*3} Marzyeh Ghassemi^{*4,1}

Abstract

Deep Metric Learning (DML) provides a crucial tool for visual similarity and zero-shot applications by learning generalizing embedding spaces, although recent work in DML has shown strong performance saturation across training objectives. However, generalization capacity is known to scale with the embedding space dimensionality. Unfortunately, high dimensional embeddings also create higher retrieval cost for downstream applications. To remedy this, we propose *Simultaneous Similarity-based Self-distillation (S2SD)*. *S2SD* extends DML with knowledge distillation from auxiliary, high-dimensional embedding and feature spaces to leverage complementary context during training while retaining test-time cost and with negligible changes to the training time. Experiments and ablations across different objectives and standard benchmarks show *S2SD* offers notable improvements of up to 7% in Recall@1, while also setting a new state-of-the-art. Code available at <https://github.com/MLforHealth/S2SD>.

1. Introduction

Deep Metric Learning (*DML*) aims to learn embedding space models in which a predefined distance metric reflects not only the semantic similarities between training samples, but also transfers to unseen classes. The generalization capabilities of these models are important for applications in image retrieval (Wu et al., 2017), face recognition (Schroff et al., 2015), clustering (Bouchacourt et al., 2018) and representation learning (He et al., 2020). Still, transfer learning into unknown test distributions remains an open problem, with Roth et al. (2020b) and Musgrave et al. (2020) revealing strong performance saturation across DML training objectives. However, Roth et al. (2020b) also show

that embedding space dimensionality can be a driver for generalization across objectives due to higher representation capacity. Indeed, this insight can be linked to recent work targeting other objective-independent improvements to DML via artificial samples (Zheng et al., 2019), higher feature distribution moments (Jacob et al., 2019) or orthogonal features (Milbich et al., 2020), which have shown promising relative improvements over selected DML objectives. Unfortunately, these methods come at a cost; be it longer training times or limited applicability. Similarly, drawbacks can be found when naively increasing the operating (*base*) dimensionality, incurring increased cost for data retrieval at test time, which is especially problematic on larger datasets. This limits realistically usable embedding dimensionalities and leads to benchmarks being evaluated against fixed, pre-defined dimensionalities.

In this work, we propose *Simultaneous Similarity-based Self-Distillation (S2SD)* to show that complex higher-dimensional information can actually be effectively leveraged in DML without changing the base dimensionality and test time cost, which we motivate from two key elements. Firstly, in DML, an additional embedding space can be spanned by a multilayer perceptron (MLP) operating over the feature representation shared with the base embedding space (see e.g. Milbich et al. (2020)). With larger dimensionalities, we can thus cheaply learn a secondary high-dimensional representation space simultaneously, also denoted as *target* embedding space. Relative to the large feature backbone, and with the *batchsize* capping the number of additional high dimensional operations, only little additional training cost is introduced. While we can not utilize the high-dimensional target embedding space at test time for aforementioned reasons, we may utilize it to boost the performance of the base embeddings.

Unfortunately, a simple connection of base and additional target embedding spaces through the shared feature backbone is insufficient for the base representation space to benefit from the auxiliary, high-dimensional information. Thus, secondly, to efficiently leverage the high-dimensional context, we use insights from knowledge distillation (Hinton et al., 2015), where a small “student” model is trained to approximate a larger “teacher” model. However, while knowledge distillation can be found in DML (Chen et al., 2018), few-shot learning (Tian et al., 2020) and self-supervised extensions thereof (Rajasegaran et al., 2020), the reliance

^{*}Equal contribution ¹University of Toronto, Vector Institute ²Heidelberg University, IWR ³Mila, Université de Montréal ⁴MIT. Correspondence to: Karsten Roth <karsten.rh1@gmail.com>.

on additional, commonly larger teacher networks or multiple training runs (Furlanello et al., 2018), introduces much higher training cost. Fortunately, we find that the target embedding space learned *simultaneously* at higher dimension can sufficiently serve as a “teacher” *during* training – through knowledge distillation of its sample similarities, the performance of the base embedding space can be improved notably. Such distillation intuitively encourages the lower-dimensional base embedding space to embed semantic similarities similar to the more expressive target embedding space and thus incorporate dimensionality-related generalization benefits.

Furthermore, *S2SD* makes use of the low cost to span additional spaces to introduce multiple teacher spaces. Operating each of them at higher, but varying dimensionality, joint distillation can then be used to enforce reusability in the distilled content akin to feature reusability in meta-learning (Raghu et al., 2020) for additional generalization boosts. Finally, in DML, the base embedding space is spanned over a penultimate feature space of much higher dimensionality, which introduces a dimensionality-based bottleneck (Milbich et al., 2020). By applying the distillation objective between feature and base embedding space in *S2SD*, we further encourage better feature usage in base embedding space. This facilitates the approximation of high-dimensional context through the base embedding space for additional improvements in generalization.

The benefits to generalization are highlighted in performance boosts across three standard benchmarks, CUB200-2011 (Wah et al., 2011), CARS196 (Krause et al., 2013) and Stanford Online Products (Oh Song et al., 2016), where *S2SD* improves test-set recall@1 of already strong DML objectives by up to 7%, while also setting a new state-of-the-art. Improvements are even more significant in very low dimensional base embedding spaces, making *S2SD* attractive for large-scale retrieval problems which can benefit from reduced embedding dimensionalities. Importantly, as *S2SD* is applied **during** the same DML training process on the **same** network backbone, no large teacher networks or additional training runs are required. Simple experiments even show that *S2SD* can outperform comparable 2-stage distillation at much lower cost.

In summary, our contributions can be described as:

- 1) We propose *Simultaneous Similarity-based Self-Distillation (S2SD)* for DML, using knowledge distillation of high-dimensional context without large additional teacher networks or training runs.
- 2) We motivate and evaluate this approach through detailed ablations and experiments, showing that the method is agnostic to choices in objectives, backbones, and datasets.
- 3) Across benchmarks, we achieve significant improvements over strong baseline objectives and state-of-the-art performance, with especially large boosts for very low-dimensional embedding spaces.

2. Related Work

Deep Metric Learning (DML) has proven useful for zero-shot image/video retrieval & clustering (Schroff et al., 2015; Wu et al., 2017; Brattoli et al., 2020), face verification (Liu et al., 2017; Deng et al., 2019) and contrastive (self-supervised) representation learning (e.g. He et al. (2020); Chen et al. (2020); Misra & van der Maaten (2020)). Approaches can be divided into **1)** improved ranking losses, **2)** tuple sampling methods and **3)** extensions to the standard DML training approach. **1)** Ranking losses place constraints on the relations available in image tuples, ranging from pairs (s.a. Hadsell et al. (2006)) to triplets (Schroff et al., 2015) and more complex orderings (Chen et al., 2017; Oh Song et al., 2016; Sohn, 2016; Wang et al., 2019). **2)** As the number of possible tuples scales exponentially with dataset size, tuple sampling approaches have been introduced to tackle tuple redundancy and to ensure that meaningful tuples are presented during training. These tuple sampling methods can follow heuristics (Schroff et al., 2015; Wu et al., 2017), be of hierarchical nature (Ge, 2018) or learned (Roth et al., 2020a). Similarly, learnable proxies to replace tuple members (Movshovitz-Attias et al., 2017; Kim et al., 2020; Qian et al., 2019) can also remedy the sampling issue, which can be extended to tackle DML from a classification viewpoint (Zhai & Wu, 2018; Deng et al., 2019). **3)** Finally, extensions to the basic training scheme can involve synthetic data (Lin et al., 2018; Zheng et al., 2019; Duan et al., 2018), complementary features (Roth et al., 2019; Milbich et al., 2020), a division into subspaces (Sanakoyeu et al., 2019; Xuan et al., 2018; Kim et al., 2018; Opitz et al., 2018), training of multiple networks (Park et al., 2020) using mutual learning (Zhang et al., 2018) or higher-order moments (Jacob et al., 2019). *S2SD* can similarly be seen as an extension to DML, though we specifically focus on capturing and distilling complex high-dimensional sample relations within lower dimensional embedding spaces to improve generalization.

Knowledge Distillation involves knowledge transfer from teacher to (usually smaller) student models, e.g. by matching network softmax outputs/logits (Buciluă et al., 2006; Hinton et al., 2015), (attention-weighted) feature maps (Romero et al., 2015; Zagoruyko & Komodakis, 2016), or latent representations (Ahn et al., 2019; Park et al., 2019; Tian et al., 2019; Laskar & Kannala, 2020). Importantly, Tian et al. (2019) show that under fair comparison, basic matching via Kullback-Leibler (KL) Divergences as used in Hinton et al. (2015) performs very well, which we also find to be the case for *S2SD*. This is further supported in recent few-shot learning literature (Tian et al., 2020), wherein KL-distillation alongside self-distillation (by iteratively reusing the same network as a teacher for beneficial generalization and regulatory properties (Furlanello et al., 2018; Lan et al., 2018; Zhang et al., 2019b; Abnar et al., 2020; Yun et al., 2020)) in additional meta-training stages improves feature

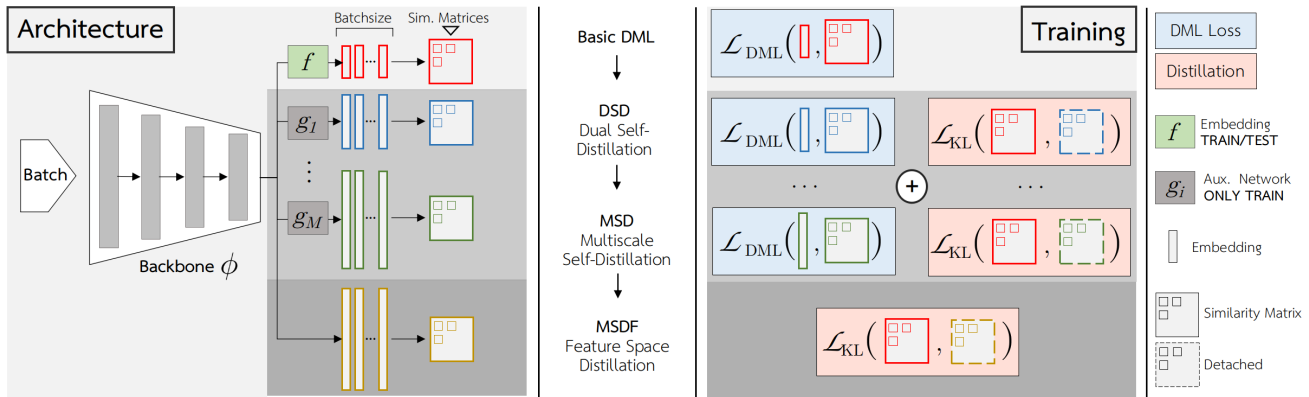


Figure 1. *S2SD*. We use a standard encoder ϕ , embedding f , and multiple auxiliary embedding networks g_i (used only during training) depending on the *S2SD* approach used. During training, for each batch of embeddings produced by the respective embedding network g_i , we compute DML losses while applying embedding distillation on the respective batch-similarity matrices (*DSD/MSD*). We further distill from the feature representation space for additional information gain (*MSDF*).

representation strength important for generalization (Raghu et al., 2020).

Our work is closest to Zhang et al. (2019a) and Liu et al. (2020), which propose to break down a network into a cascading set of subnetworks, wherein each subsequent subnetwork builds on its predecessors. In doing so, each subnetwork is trained independently on a classification task at hand. Knowledge distillation is then applied either from the full network (Zhang et al., 2019a) acting as a teacher or via soft targets generated from a meta-learned label generator (Liu et al., 2020), to each smaller student subnetwork during the same training run to improve overall performance. In a related manner, *S2SD* utilizes similar concurrent, but relational self-distillation to instead encode high-dimensional sample relation context from multiple, higher-dimensional teacher embedding spaces; this is crucial to improve the generalization capabilities of a single student embedding space for zero-shot, out-of-distribution image retrieval tasks. As such, it operates orthogonally to proposals made by Zhang et al. (2019a) and Liu et al. (2020). The concurrency of the self-distillation in turn is a consequence of the novel insight that solely the dimensionality of embedding spaces can serve as meaningful teachers, as these can be spanned cheaply over a large, shared feature backbone.

The novel dimensionality-based concurrent distillation also sets *S2SD* apart from existing knowledge distillation applications to DML, which are done in a generic manner with separate, larger teacher networks or additional training stages (Chen et al., 2018; Yu et al., 2019; Han et al., 2019; Laskar & Kannala, 2020).

3. Method

We now introduce key elements for *Simultaneous Similarity-based Self-Distillation (S2SD)* to improve generalization of embedding spaces by utilizing higher dimensional context. We begin with the preliminary notation and fundamentals to Deep Metric Learning (§3.1), before defining the three key elements to *S2SD*: Firstly, the Dual Self-Distillation (DSD) objective, which uses KL-Distillation on a concurrently learned embedding space of higher dimensionality (§3.2) to introduce important high-dimensional context into a low-dimensional embedding space during training. We then extend this to Multiscale Self-Distillation (MSD) with distillation from several different high-dimensional embedding spaces to encourage reusability in the distilled context (§3.3). Finally, we shift to self-distillation from normalized feature representations (MSDF) to counter dimensionality bottlenecks commonly encountered in DML (§3.4).

3.1. Preliminaries

DML builds on generic Metric Learning which aims to find a (parametrized) distance metric $d_\theta : \Phi \times \Phi \mapsto \mathbb{R}$ on the *feature space* $\Phi \subset \mathbb{R}^{d^*}$ over images \mathcal{X} that best satisfy ranking constraints usually defined over class labels \mathcal{Y} . This holds also for DML. However, while Metric Learning relies on a **fixed** feature extraction method to obtain Φ , DML introduces deep neural networks to concurrently learn a feature representation. Most such DML approaches aim to learn Mahalanobis distance metrics, which cover the parametrized family of inner product metrics (Suárez et al., 2018; Chen et al., 2019). These metrics, with some restrictions (Suárez

et al., 2018), can be reformulated as

$$\begin{aligned} d(\phi_1, \phi_2) &= \sqrt{(L(\phi_1 - \phi_2))^T L(\phi_1 - \phi_2)} \\ &= \|L\phi_1 - L\phi_2\|_2 = \|\psi_1 - \psi_2\|_2 \end{aligned} \quad (1)$$

with learned linear projection $L \in \mathbb{R}^{d \times d^*}$ from d^* -dim. features $\phi_i \in \Phi$ to d -dim. embeddings $\psi_i := (f \circ \phi)(x_i) \in \Psi_f$ with embedding function $f : \phi_i \mapsto L\phi_i$. Importantly, this redefines the motivation behind DML as learning d -dimensional image embeddings ψ s.t. their euclidean distance $d(\bullet, \bullet) = \|\bullet - \bullet\|_2$ is connected to semantic similarities in \mathcal{X} . This embedding-based formulation offers the significant advantage of being compatible with fast approximate similarity search methods (e.g. (Johnson et al., 2017)), allowing for large-scale applications at test time. In this work, we assume Ψ_f to be normalized to the unit hypersphere \mathcal{S}_{Ψ_f} , which is commonly done (Wu et al., 2017; Sanakoyeu et al., 2019; Liu et al., 2017; Wang & Isola, 2020) for beneficial regularizing purposes (Wu et al., 2017; Wang & Isola, 2020). For the remainder we hence set Ψ to refer to \mathcal{S}_{Ψ} .

Common approaches to learn such a representation space involve training surrogates on ranking constraints defined by class labels. Such approaches start from pair or triplet-based ranking objectives (Hadsell et al., 2006; Schroff et al., 2015), where the latter is defined as

$$\mathcal{L}_{\text{triplet}} = \frac{1}{|\mathcal{T}_{\mathcal{B}}|} \sum_{(x_i, x_j, x_k) \in \mathcal{T}_{\mathcal{B}}} [d(\psi_i, \psi_j) - d(\psi_i, \psi_k) + m]_+ \quad (2)$$

with margin m and the set of available triplets $(x_i, x_j, x_k) \in \mathcal{T}_{\mathcal{B}}$ in a mini-batch $\mathcal{B} \subset \mathcal{X}$, with $y_i = y_j \neq y_k$. This can be extended with more complex ranking constraints or tuple sampling methods. We refer to Supp. B and Roth et al. (2020b) for further insights and detailed studies.

3.2. Embedding Space Self-Distillation

For the aforementioned standard DML setting, generalization performance of a learned embedding space can be linked to the utilized embedding dimensionality. However, high dimensionality results in notably higher retrieval cost on downstream applications, which limits realistically usable dimensions. In *S2SD*, we show that high-dimensional context can be used as a teacher during the training run of the low-dimensional *base* or *reference* embedding space. As the base embedding model is also the one that is evaluated, test time retrieval costs are left unchanged.

To achieve this, we simultaneously train an additional high-dimensional *auxiliary/target* embedding space $\Psi_g := (g \circ \phi)(\mathcal{X})$ spanned by a secondary embedding branch g . g is parametrized by a MLP or a linear projection, similar to the base embedding space Ψ_f spanned by f , see §3.1. Both f

and g operate on the same large, shared feature backbone ϕ . For simplicity, we train Ψ_f and Ψ_g using the same DML objective \mathcal{L}_{DML} .

Unfortunately, higher expressivity and improved generalization of high-dimensional embeddings in Ψ_g hardly benefit the base embedding space, even with a shared feature backbone. To explicitly leverage high-dimensional context for our base embedding space, we utilize knowledge distillation from target to base space. However, while common knowledge distillation approaches match single embeddings or features between student and teacher, the different dimensionalities in Ψ_f and Ψ_g inhibit naive matching.

Instead, *S2SD* matches sample relations (see e.g. (Tian et al., 2019)) defined over batch-similarity matrices $D \in \mathbb{R}^{\mathcal{B} \times \mathcal{B}}$ in base and target space, D^f and D^g , with batchsize \mathcal{B} . We thus encourage the base embedding space to relate different samples in a similar manner to the target space. To compute D , we use a cosine similarity by default, given as $D_{i,j} = \psi_i^T \psi_j$, since ψ_i is normalized to the unit hypersphere. Defining σ_{\max} as the softmax operation and $\mathcal{D}_{\text{KL}}(p, q) = \sum \log(p)^{\log(p)/\log(q)}$ as the Kullback-Leibler divergence, we thus define the simultaneous self-distillation objective as

$$\mathcal{L}_{\text{dist}}(D^f, D^g) = \sum_i^{|\mathcal{B}|} \mathcal{D}_{\text{KL}} \left(\sigma_{\max} (D_{i,:}^f / T), \sigma_{\max} (D_{i,:}^g / T) \right) \quad (3)$$

with temperature T , as visualized in Figure 1. (\dagger) denotes no gradient flow to target branches g as we only want the base space to learn from the target space. By default, we match rows or columns of D , $D_{i,:}$, effectively distilling the relation of an anchor embedding ψ_i to all other batch samples. Embedding all batch samples in base dimension, $\Psi_f^{\mathcal{B}} : \mathcal{B} \mapsto \psi_f(\mathcal{B})$, and higher dimension, $\Psi_g^{\mathcal{B}} : \mathcal{B} \mapsto \psi_g(\mathcal{B})$, the (simultaneous) *Dual Self-Distillation* (DSD) training objective then becomes

$$\begin{aligned} \mathcal{L}_{\text{DSD}}(\Psi_f^{\mathcal{B}}, \Psi_g^{\mathcal{B}}) &= 1/2 \cdot [\mathcal{L}_{\text{DML}}(\Psi_f^{\mathcal{B}}) + \mathcal{L}_{\text{DML}}(\Psi_g^{\mathcal{B}})] \\ &\quad + \gamma \cdot \mathcal{L}_{\text{dist}}(D^f, D^g) \end{aligned} \quad (4)$$

3.3. Reusable Relations by Multiscale Distillation

While *DSD* encourages the reference embedding space to recover complex sample relations by distilling from a higher-dimensional target space spanned by g , it is not known *a priori* which distillable sample relations actually benefit generalization of the reference space.

To encourage the usage of sample relations that more likely aid generalization, we follow insights made in Raghu et al. (2020) on the connection between **reusability** of features across multiple tasks and better generalization thereof. We motivate reusability in *S2SD* by extending *DSD* to *Multiscale Self-Distillation* (*MSD*) with distillation instead from m multiple different target spaces spanned

by $G = \{g_k\}_{k \in \{1, m\}}$. Importantly, each of these high-dimensional target spaces operate on different dimensionalities, i.e. $\dim f < \dim g_1 < \dots < \dim g_{m-1} < \dim g_m$. As this results in each target embedding space encoding sample relations differently, application of distillation across all spaces spanned by G pushes the base branch towards learning from sample relations that are reusable across all higher dimensional embedding spaces and thereby more likely to generalize (see also Fig. 1).

Specifically, given the set of target similarity matrices $\{D^k\}_{k \in \{f, g_1, \dots, g_m\}}$ and target batch embeddings $\Gamma^m := \{\Psi_k^B\}_{k \in \{f, g_1, \dots, g_m\}}$, we then define the *MSD* training objective as

$$\begin{aligned} \mathcal{L}_{\text{MSD}}(\Gamma^m) = & \frac{1}{2} \cdot \left[\mathcal{L}_{\text{DML}}(\Psi_f^B) + \frac{1}{m} \sum_{i=1}^m \mathcal{L}_{\text{DML}}(\Psi_{g_i}^B) \right] \\ & + \frac{\gamma}{m} \sum_{i=1}^m \mathcal{L}_{\text{dist}}(D^f, D^{g_i}) \end{aligned} \quad (5)$$

3.4. Tackling the Dimensionality Bottleneck by Feature Space Self-Distillation

As noted in §3.1, the base embedding Ψ utilizes linear projections f from the (penultimate) feature space Φ where $\dim \Phi$ is commonly much larger than $\dim \Psi$. While compressed semantic spaces encourage stronger representations (Alemi et al., 2016; Dai & Wipf, 2019) to be learned, Milbich et al. (2020) show that the actual test performance of the lower-dimensional embedding space Φ is inferior to that of the non-adapted, but higher-dimensional feature space Ψ .

This supports a dimensionality-based loss of information beneficial to generalization, which can hinder the base embedding space to optimally approximate the high-dimensional context introduced in §3.2 and 3.3.

To rectify this, we apply self-distillation following eq. 3 on the normalized feature representations Φ^n generated by normalizing the backbone output ϕ . With the batch of normalized feature representations $\Psi_{\phi^n}^B$ we get *multiscale self-distillation with feature distillation (MSDF)* (see also Fig. 1)

$$\mathcal{L}_{\text{MSDF}}(\Gamma^m, \Psi_{\phi^n}^B) = \mathcal{L}_{\text{MSD}}(\Gamma^m) + \gamma \mathcal{L}_{\text{dist}}(D^f, D^{\phi^n}) \quad (6)$$

In the same manner, one can also address other architectural information bottlenecks such as through the generation of feature representations from a single global pooling operation. While not noted in the original publication, Kim et al. (2020) address this in the official code release by using both global max- and average pooling to create their base embedding space. While this naive usage changes the architecture at test time, in *S2SD* we can *fairly* leverage potential benefits by *only* spanning the auxiliary spaces (and distilling) from such feature representations (denoted as *DSDA/MSDA/MSDFA*).

4. Experimental Setup

We study *S2SD* in four experiments to establish 1) method ablation performance & relative improvements, 2) state-of-the-art, 3) comparisons to standard 2-stage distillation, benefits to low-dimensional embedding spaces & generalization properties and 4) motivation for architectural choices.

Method Notation. We abbreviate ablations of *S2SD* (see §3) in our experiments as: *DSD* & *MSD* for **Dual** (3.2) & **Multiscale Self-Distillation** (3.3), *MSDF* the addition of *Feature distillation* (3.4) and *DSDA/MSD(F)* the inclusion of multiple pooling operations in the auxiliary branches (also §3.4).

4.1. Experiments

Fair Evaluation of *S2SD*. §5.1 specifically applies *S2SD* and its ablations to three DML baselines. To show realistic benefit, *S2SD* is applied to best-performing objectives evaluated in Roth et al. (2020b), namely (i) Margin loss with Distance-based Sampling (Wu et al., 2017), (ii) their proposed Regularized Margin loss and (iii) Multisimilarity loss (Wang et al., 2019), following their experimental training pipeline. This setup utilizes no learning rate scheduling and fixes common implementational factors of variation in DML pipelines such as batchsize, base embedding dimension, weight decay or feature backbone architectures to ensure comparability in DML (more details in Supp. A.2). As such, our results are directly comparable to their large set of examined methods and guaranteed that relative improvements solely stem from the application of *S2SD*.

Comparison to literature. §5.2 further highlights the benefits of *S2SD* by comparing *S2SD*'s boosting properties across literature standards, with different backbone architectures and base embedding dimensions: (1) ResNet50 with $d = 128$ (Wu et al., 2017; Roth et al., 2019) and (2) $d = 512$ (Zhai & Wu, 2018) as well as (3) variants to Inception-V1 with Batch-Normalization at $d = 512$ (Wang et al., 2019; Qian et al., 2019; Milbich et al., 2020). Only here do we conservatively apply learning rate scheduling, since all references noted in Table 2 employ scheduling as well. We categorize published work based on backbone architecture and embedding dimension for fairer comparison. Note that this is a less robust comparison than done in §5.1, due to potential implementation differences between our pipeline and reported literature results.

Comparison to 2-Stage Distillation. §5.3 compares *S2SD* to 2-stage distillation, investigates benefits to very low dimensional reference spaces and examines the connection between improvements and changes in embedding space density and spectral decay (see Supp. D), which have been linked to improved generalization.

Ablation Study. §5.4 ablates and motivates architectural

Table 1. *S2SD* comparison against strong baseline objectives. **Bold** denotes best results per objective, **bluebold** marks best overall results. mAP@R results as proposed in (Roth et al., 2020b) and (Musgrave et al., 2020) as well as ProxyAnchor evaluations (Kim et al. (2020), using a different setup) can be found in the Supplementary (Table 5 and 6), further showing the notable benefits of *S2SD*.

BENCHMARKS→	CUB200-2011		CARS196		SOP	
APPROACHES ↓	R@1	NMI	R@1	NMI	R@1	NMI
Margin , $\beta = 1.2$, (Wu et al., 2017)	63.09 ± 0.46	68.21 ± 0.33	79.86 ± 0.33	67.36 ± 0.34	78.43 ± 0.07	90.40 ± 0.03
+ DSD	65.11 ± 0.18	69.65 ± 0.44	83.19 ± 0.18	69.28 ± 0.56	79.05 ± 0.12	90.52 ± 0.18
+ MSD	66.13 ± 0.34	70.83 ± 0.27	83.63 ± 0.31	69.80 ± 0.36	79.26 ± 0.15	90.60 ± 0.10
+ MSDF	67.58 ± 0.32	71.47 ± 0.19	85.55 ± 0.23	71.68 ± 0.54	79.63 ± 0.15	90.70 ± 0.09
+ MSDFA	67.21 ± 0.23	71.43 ± 0.25	86.45 ± 0.35	71.46 ± 0.24	78.82 ± 0.09	90.49 ± 0.06
R-Margin , $\beta = 0.6$, (Roth et al., 2020b)	64.93 ± 0.42	68.36 ± 0.32	82.37 ± 0.13	68.66 ± 0.47	77.58 ± 0.11	90.42 ± 0.03
+ DSD	66.58 ± 0.08	70.03 ± 0.41	84.64 ± 0.16	70.87 ± 0.18	77.86 ± 0.10	90.50 ± 0.03
+ MSD	66.81 ± 0.27	70.47 ± 0.16	85.01 ± 0.10	71.67 ± 0.40	78.00 ± 0.06	90.47 ± 0.04
+ MSDF	68.12 ± 0.30	71.80 ± 0.33	85.78 ± 0.22	72.24 ± 0.31	78.57 ± 0.09	90.58 ± 0.02
+ MSDFA	68.58 ± 0.26	71.64 ± 0.40	86.81 ± 0.35	71.48 ± 0.29	78.00 ± 0.11	90.41 ± 0.02
Multisimilarity (Wang et al., 2019)	62.80 ± 0.70	68.55 ± 0.38	81.68 ± 0.19	69.43 ± 0.38	77.99 ± 0.09	90.00 ± 0.02
+ DSD	65.57 ± 0.26	70.08 ± 0.33	83.51 ± 0.20	70.30 ± 0.05	78.23 ± 0.04	90.08 ± 0.04
+ MSD	65.80 ± 0.16	70.66 ± 0.01	83.98 ± 0.10	71.34 ± 0.09	78.42 ± 0.09	90.09 ± 0.03
+ MSDF	67.04 ± 0.29	71.87 ± 0.19	85.69 ± 0.19	72.77 ± 0.13	78.59 ± 0.08	90.09 ± 0.06
+ MSDFA	67.68 ± 0.29	71.40 ± 0.21	85.89 ± 0.15	71.45 ± 0.26	78.07 ± 0.06	89.88 ± 0.10

choices in *S2SD* used throughout §4. Pseudo code and detailed results are available in Supp. F, G, and I.

4.2. Implementation

Datasets & Evaluation. In all experiments, we evaluate on standard DML benchmarks: *CUB200-2011* (Wah et al., 2011), *CARS196* (Krause et al., 2013) and *Stanford Online Products (SOP)* (Oh Song et al., 2016). Performance is measured in *recall at 1* (R@1) and *at 2* (R@2) (Jegou et al., 2011) as well as *Normalized Mutual Information* (NMI) (Manning et al., 2010). Results measured on mean Average Precision evaluated on Recall (mAP@R) are available in the Supplementary along with additional dataset details.

Experimental Details. Our implementation follows Roth et al. (2020b) for comparability, using frozen Batch-Normalization (Ioffe & Szegedy, 2015) whenever a ResNet50 (He et al., 2016) is utilized, Adam (Kingma & Ba, 2015) with learning rate 10^{-5} for training and weight decay (Krogh & Hertz, 1992) of $4 \cdot 10^{-5}$ for regularization. Additional details are available in Supp. (A). For §5.1-5.4, we only adjust the respective pipeline elements in questions. For *S2SD*, unless noted otherwise (s.a. in §5.4), we set $\gamma = 50$, $T = 1$ for all objectives on CUB200 and CARS196, and $\gamma = 5$, $T = 1$ on SOP. *DSD* uses target-dim. $d = 2048$ and *MSD* uses target-dims. $d \in [512, 1024, 1536, 2048]$. We found it beneficial to activate the feature distillation after $n = 1000$ iterations to ensure that meaningful features are learned first before feature distillation is applied. Additional embedding spaces are spanned by two layer MLPs with row-wise KL-distillation of high-dimensional similarities (eq. 3), applied as in $\mathcal{L}_{\text{multi}}$ (eq. 5). By default, we use Multisimilarity Loss as stand-in for \mathcal{L}_{DML} . Hyperpa-

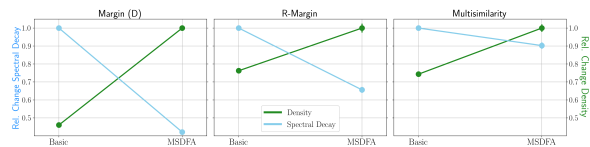


Figure 2. Generalization metrics. *S2SD* increases embedding space density and lowers spectral decay.

rameters were determined previous to the result runs using a 80-20 training and validation split, similar to Roth et al. (2020b) and Kim et al. (2020).

5. Results

5.1. Fair performance study

In Tab. 1 (full table in Supp. Tab. 4), we show that under fair experimental protocol, utilizing *S2SD* and its ablations gives an objective and benchmark independent, significant boost in performance by up to 7% opposing the existing DML objective performance plateau. This holds even for previous state-of-the-art regularized objectives s.a. R-Margin loss as well as proxy-based objectives such as ProxyAnchor (Kim et al. (2020), see Supplementary), highlighting the effectiveness of *S2SD* for DML. Across objectives, *S2SD*-based changes in wall-time do not exceed negligible 5% with only minor convergence impacts.

5.2. Setting a new State-of-the-Art

Motivated by Tab. 1, we use *MSDFA* for CUB200/CARS196 and *MSDF* for SOP. Table 2 shows that *S2SD* can boost baseline objectives to reach and even surpass other state-of-the-

Table 2. *State-of-the-art comparison.* We show that *S2SD*, represented by its variants *MSDF(A)*, boosts baseline objectives to state-of-the-art across literature. (*) stands for Inception-V1 with frozen Batch-Norm. **Bold**: best results per literature setup. **Bluebold**: best results per overall benchmark.

BENCHMARKS →	CUB200 (Wah et al., 2011)			CARS196 (Krause et al., 2013)			SOP (Oh Song et al., 2016)		
METHODS ↓	R@1	R@2	NMI	R@1	R@2	NMI	R@1	R@10	NMI
ResNet50-128									
Div&Conq (Sanakoyeu et al., 2019)	65.9	76.6	69.6	84.6	90.7	70.3	75.9	88.4	90.2
MIC (Roth et al., 2019)	66.1	76.8	69.7	82.6	89.1	68.4	77.2	89.4	90.0
PADS (Roth et al., 2020a)	67.3	78.0	69.9	83.5	89.7	68.8	76.5	89.0	89.9
Multisimilarity+S2SD	68.0 ± 0.2	78.7 ± 0.1	71.7 ± 0.4	86.3 ± 0.1	91.8 ± 0.3	72.0 ± 0.3	79.0 ± 0.2	90.2 ± 0.1	90.6 ± 0.1
Margin+S2SD	67.6 ± 0.3	78.2 ± 0.2	70.8 ± 0.3	86.0 ± 0.2	91.8 ± 0.2	72.2 ± 0.2	80.2 ± 0.2	91.5 ± 0.1	90.9 ± 0.1
R-Margin+S2SD	68.9 ± 0.3	79.0 ± 0.3	72.1 ± 0.4	87.6 ± 0.2	92.7 ± 0.2	72.3 ± 0.2	79.2 ± 0.2	90.3 ± 0.1	90.8 ± 0.1
ResNet50-512									
EPSHN (Xuan et al., 2020)	64.9	75.3	-	82.7	89.3	-	78.3	90.7	-
NormSoft (Zhai & Wu, 2018)	61.3	73.9	-	84.2	90.4	-	78.2	90.6	-
DiVA (Milbich et al., 2020)	69.2	79.3	71.4	87.6	92.9	72.2	79.6	91.2	90.6
Multisimilarity+S2SD	69.2 ± 0.1	79.1 ± 0.2	71.4 ± 0.2	89.2 ± 0.2	93.8 ± 0.2	74.0 ± 0.2	80.8 ± 0.2	92.2 ± 0.2	90.5 ± 0.3
Margin+S2SD	68.8 ± 0.2	78.5 ± 0.2	72.3 ± 0.1	89.3 ± 0.2	93.8 ± 0.2	73.7 ± 0.3	81.0 ± 0.2	92.1 ± 0.2	91.1 ± 0.3
R-Margin+S2SD	70.1 ± 0.2	79.7 ± 0.2	71.6 ± 0.2	89.5 ± 0.2	93.9 ± 0.3	72.9 ± 0.3	80.0 ± 0.2	91.4 ± 0.2	90.8 ± 0.1
Inception-BN-512									
DiVA (Milbich et al., 2020)	66.8	77.7	70.0	84.1	90.7	68.7	78.1	90.6	90.4
Multisimilarity+S2SD	66.7 ± 0.3	77.5 ± 0.3	70.5 ± 0.2	83.8 ± 0.3	90.3 ± 0.2	69.8 ± 0.3	78.5 ± 0.2	90.6 ± 0.2	90.6 ± 0.1
Margin+S2SD	66.8 ± 0.2	77.9 ± 0.2	69.9 ± 0.3	84.3 ± 0.2	90.7 ± 0.2	69.8 ± 0.2	78.4 ± 0.2	90.5 ± 0.2	90.4 ± 0.1
R-Margin+S2SD	67.4 ± 0.3	78.0 ± 0.4	70.3 ± 0.2	83.9 ± 0.3	90.3 ± 0.2	69.4 ± 0.2	78.1 ± 0.2	90.4 ± 0.3	90.3 ± 0.2
Softtriple* (Qian et al., 2019)	65.4	76.4	69.3	84.5	90.7	70.1	78.3	90.3	92.0
Multisimilarity* (Wang et al., 2019)	65.7	77.0	-	84.1	90.4	-	78.2	90.5	-
Multisimilarity*+S2SD	68.2 ± 0.3	79.1 ± 0.2	71.6 ± 0.2	86.3 ± 0.2	92.2 ± 0.2	72.0 ± 0.3	78.9 ± 0.2	90.8 ± 0.2	90.6 ± 0.1
Margin*+S2SD	68.3 ± 0.2	78.8 ± 0.2	71.2 ± 0.2	87.1 ± 0.2	92.4 ± 0.1	72.2 ± 0.2	79.1 ± 0.2	91.0 ± 0.3	90.4 ± 0.1
R-Margin*+S2SD	69.6 ± 0.3	79.6 ± 0.3	71.2 ± 0.1	86.6 ± 0.3	92.1 ± 0.3	70.9 ± 0.2	78.5 ± 0.1	90.5 ± 0.2	90.0 ± 0.2

art methods, in parts with a notable margin. This holds even when compared to much more complex methods with feature mining or RL-policies such as MIC (Roth et al., 2019), DiVA (Milbich et al., 2020) or PADS (Roth et al., 2020a), to which *S2SD* operates orthogonally. Finally, we note that these insights are true even with our results reported with confidence intervals, which is commonly neglected in DML.

5.3. Benefits of S2SD

Comparison to standard distillation. With a student S using the same objective and embedding dimensionality as the reference branch in *DSD* and a teacher T at the highest optimal dimensionality $d = 2048$, we find that separating *DSD* into a standard 2-stage distillation setup actually degenerates performance (see Fig. 3A, compare to *Dist.*). In addition, *S2SD* allows for easy integration of teacher ensembles, realized by *MSDF(A)*, to even outperform the teacher by a notable margin. This is specifically interesting as *S2SD* retains the operating embedding dimensionality of the student.

Benefits to lower base dimensions. We now show that our module is able to vastly boost networks limited to very low embedding dimensions, which we visualize in figure 3B). For example, networks operating on $d = 32$ & 64 trained with *S2SD* can match the performance of networks trained

and evaluated on embedding dimensions *four or eight times* the size. For $d = 128$, *S2SD* even outperforms the highest dimensional baseline at $d = 2048$ by a large margin.

Embedding space metrics. We now look at relative changes in embedding space density and spectral decay (see supplementary of Roth et al. (2020b)) when applying *S2SD*. Our study, visualized in figure 2, shows that the application of *S2SD* increases embedding space density and lowers the spectral decay (thus providing a more feature-diverse embedding space) across criteria, which is aligned with properties of improved generalization in DML as noted in Roth et al. (2020b).

5.4. Motivating S2SD Architecture Choices

Distillation improves generalization through S2SD. Fig. 3A (*Joint*) and Fig. 3F ($\gamma = 0$) highlight how crucial self-distillation is, as incorporating a secondary embedding space without any distillation link hardly improves performance. Fig. 3A (*Concur.*) further shows that joint training of a detached reference embedding f , while otherwise training in high dimension, similarly doesn't offer notable improvement. Finally, Figure 3F shows robustness to changes in γ , with peaks around $\gamma = 50$ and $\gamma = 5$ for CUB200/CARS196 and SOP. We also found best performance for temperatures $T \in [0.2, 2]$ and hence set $T = 1$

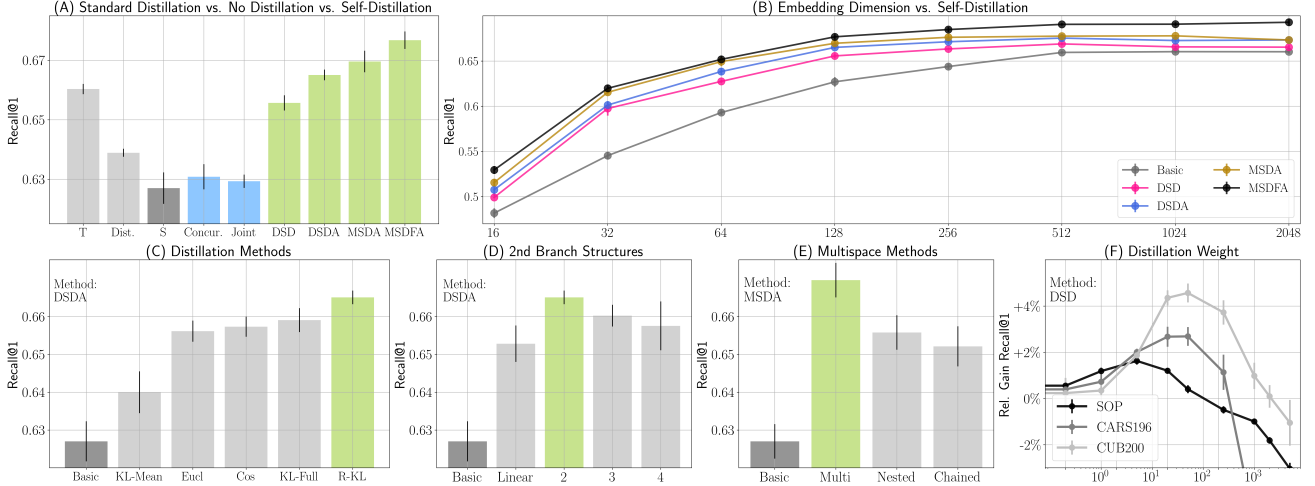


Figure 3. *S2SD* study and ablations. (A) *DSD* outperforms comparable two-stage distillation on student S (*Dist.*) using teacher (T), with *MSD(FA)* even outperforming T . We further see that distillation is essential - training multiple spaces in parallel (*Joint.*) or a detached lower-dimensional base embedding (*Concur.*) gives little benefit. (B) We see benefits across base dimensionalities, especially in the low-dimensional regime. (C) We find KL-distillation between similarity vectors (*R-KL*) to work best. (D) An additional non-linearity in aux. branches g gives a boost, but going deeper hurts generalization. (E) Distilling each aux. embed. space (*Multi*) separately compares favourable against other distillation setups s.a. *Nested* and *Chained* distillation. (F) Performance is robust to changes in weight values.

by default.

Best way to enforce reusability. To motivate our many-to-one self-distillation \mathcal{L}_{MSD} (eq. 5, here also dubbed $\mathcal{L}_{\text{Multi}}$), we evaluate against other distillation setups that could support reusability of distilled sample relations: (1) *Nested* distillation, where instead of distilling all target spaces only to the reference space, we distill from a target space to *all* lower-dimensional embedding spaces:

$$\begin{aligned} \mathcal{L}_{\text{Nested}}(\Gamma^m) = & \frac{1}{2} \left[\mathcal{L}_{\text{DML}}(\Psi_f^{\mathcal{B}}) + \frac{1}{m} \sum_{i=1}^m \mathcal{L}_{\text{DML}}(\Psi_{g_i}^{\mathcal{B}}) \right] \\ & + \frac{\gamma}{\binom{m}{m-1}} \sum_{\substack{i=0, j=1, j \neq i \\ \dim g_j \geq \dim g_i}}^m \mathcal{L}_{\text{dist}}(\Psi_{g_i}^{\mathcal{B}}, \Psi_{g_j}^{\mathcal{B}}) \end{aligned} \quad (7)$$

In the second term, g_0 denotes the base embedding f . (2) *Chained* distillation, which distills target spaces only to the immediate lower-dimensional embedding space:

$$\begin{aligned} \mathcal{L}_{\text{Chained}}(\Gamma^m) = & \frac{1}{2} \left[\mathcal{L}_{\text{DML}}(\Psi_f^{\mathcal{B}}) + \frac{1}{m} \sum_{i=1}^m \mathcal{L}_{\text{DML}}(\Psi_{g_i}^{\mathcal{B}}) \right] \\ & + \frac{\gamma}{m} \sum_{i=1}^{m-1} \mathcal{L}_{\text{dist}}(\Psi_{g_i}^{\mathcal{B}}, \Psi_{g_{i-1}}^{\mathcal{B}}) \end{aligned} \quad (8)$$

Figure 3E shows that a many-to-one distillation performs notably better, supporting the reusability aspect and $\mathcal{L}_{\text{multi}}$ as our default method.

Choice of distillation method & branch structures. Fig. 3C evaluates various distillation objectives, finding KL-divergence between vectors of similarities to perform better than KL-divergence applied over full similarity matrices or row-wise means thereof, as well as cosine/euclidean distance-based distillation (see e.g. Yu et al. (2019)). Figure 3D shows insights into optimal auxiliary branch structures, with two-layer MLPs giving the largest benefit, although even a linear target mapping reliably boosts performance. This coincides with insights made by Chen et al. (2020). Further network depth only deteriorates performance.

6. Conclusion

In this paper, we propose a novel DML training paradigm based on dimensionality-based knowledge distillation, *Simultaneous Similarity-based Self-Distillation (S2SD)*. *S2SD* allows for the inclusion of reusable, context-rich, high-dimensional relational information for improved generalization. This is achieved by solving the standard DML objective simultaneously in higher-dimensional embedding spaces while applying knowledge distillation concurrently between these high-dimensional teacher spaces and a lower-dimensional reference space. In doing so, *S2SD* introduces little additional computational overhead, with no extra cost at test time. Thorough ablations and experiments show *S2SD* significantly improving the generalization performance of existing DML objectives regardless of embedding dimensionality, thereby also setting a new state-of-the-art.

Acknowledgements

We would like to thank Samarth Sinha (University of Toronto, Vector), Matthew McDermott (MIT) and Mengye Ren (University of Toronto, Vector) for insightful discussions and feedback on the paper draft. This work was funded in part by a CIFAR AI Chair at the Vector Institute, Microsoft Research, and an NSERC Discovery Grant. Resources used in preparing this research were provided, in part, by the Province of Ontario, the Government of Canada through CIFAR, and companies sponsoring the Vector Institute www.vectorinstitute.ai/#partners.

Reviewer Comments

Re: More advanced baseline methods. We do believe that our reported results are representative of the current state of Deep Metric Learning - under fair comparison (Roth et al., 2020b), Multisimilarity and Margin loss achieve best or competitive results. In addition, *S2SD* is applied to regularized Deep Metric Learning (R-Margin loss (Roth et al., 2020b)) and shows high improvements throughout. ProxyAnchor (Kim et al., 2020) was not included in the literature comparison due to different architecture settings (lines 268-271), thus not allowing for a fair comparison. DiVA in turn offers a separate extension to DML and should be seen as orthogonal to *S2SD*, which however we consistently outperform. However, for completeness, we have applied *S2SD* to ProxyAnchor using the fair comparison setup in Roth et al. (2020b) (see section 5.1) on all benchmarks to highlight the general applicability of *S2SD*. We perform no hyperparameter tuning and use those already mentioned in the paper and find notable and consistent performance improvements. Results are available in the supplementary (Table 6).

Re: Runtime Analysis. We offer a dimensionality versus runtime analysis in the supplementary (Table 3), which shows significant runtime reduction by up to a magnitude: With performance of $d = 64$ roughly matching that of $d = 2048$, retrieval runtime on $N = 250000$ synthetic evaluation samples can be reduced from 27.21 ± 0.17 to 1.98 ± 0.00 seconds. The high performance boost also offers the benefit of reduced memory storage needed to retain embedding vectors for comparable retrieval performance.

Re: Necessity of loss terms. There are only three effective loss terms. Firstly, the default DML objective \mathcal{L}_{DML} applied to each branch. Secondly, the actual distillation objective over all branches $\frac{\gamma}{m} \sum_{i=1}^m \mathcal{L}_{\text{Dist}}(D^f, D^{g^i})$ (see eq. 5) and thirdly, the feature space self-distillation to counter the dimensionality bottleneck (see eq. 6). These last two correspond to the *S2SD* variants MSD and MSDF, which we evaluate against different variants of \mathcal{L}_{DML} in section 5.1. As can be seen, both loss-terms operate complementary. Regarding general convergence behaviour and training

dynamics, we find only minor changes, with maximum performance achieved at similar training stages.

Re: Validation Information. All benchmarks only offer a train/test split. As such, we use a 80-20 train/validation split of the original training split to determine hyperparameters (e.g. Roth et al. (2020b) and Kim et al. (2020)), and use those for training on the full training dataset and evaluation on the test set used throughout literature (see Sec. 4).

Re: Theoretical Grounding. While we do not offer detailed theoretical formalism in this paper as to why *S2SD* is so effective, we do evaluate changes in the embedding space structure (see figure 2), which highlight that *S2SD* encourages noticeably higher feature diversity and embedding space uniformity linked to improved generalization (Roth et al., 2020b; Wang & Isola, 2020; Milbich et al., 2020).

References

- Abnar, S., Dehghani, M., and Zuidema, W. H. Transferring inductive biases through knowledge distillation. *CoRR*, abs/2006.00555, 2020. URL <https://arxiv.org/abs/2006.00555>.
- Ahn, S., Hu, S. X., Damianou, A., Lawrence, N. D., and Dai, Z. Variational information distillation for knowledge transfer. *2019 IEEE/CVF Conference on Computer Vision and Pattern Recognition (CVPR)*, Jun 2019. doi: 10.1109/cvpr.2019.00938. URL <http://dx.doi.org/10.1109/CVPR.2019.00938>.
- Alemi, A. A., Fischer, I., Dillon, J. V., and Murphy, K. Deep variational information bottleneck. *CoRR*, abs/1612.00410, 2016. URL <http://arxiv.org/abs/1612.00410>.
- Bouchacourt, D., Tomioka, R., and Nowozin, S. Multi-level variational autoencoder: Learning disentangled representations from grouped observations. In *AAAI 2018*, 2018.
- Brattoli, B., Tighe, J., Zhdanov, F., Perona, P., and Chalupka, K. Rethinking zero-shot video classification: End-to-end training for realistic applications. In *Proceedings of the IEEE/CVF Conference on Computer Vision and Pattern Recognition (CVPR)*, June 2020.
- Bucilua, C., Caruana, R., and Niculescu-Mizil, A. Model compression. In *Proceedings of the 12th ACM SIGKDD international conference on Knowledge discovery and data mining*, pp. 535–541, 2006.
- Chen, S., Luo, L., Yang, J., Gong, C., Li, J., and Huang, H. Curvilinear distance metric learning. In *Advances in Neural Information Processing Systems 32*, pp. 4223–4232. Curran Associates, Inc., 2019. URL <http://papers.nips.cc/paper/>

- 8675-curvilinear-distance-metric-learning.pdf. *conference on computer vision and pattern recognition*, pp. 770–778, 2016.
- Chen, T., Kornblith, S., Norouzi, M., and Hinton, G. E. A simple framework for contrastive learning of visual representations. 2020. URL <https://arxiv.org/abs/2002.05709>.
- Chen, W., Chen, X., Zhang, J., and Huang, K. Beyond triplet loss: a deep quadruplet network for person re-identification. In *Proceedings of the IEEE Conference on Computer Vision and Pattern Recognition*, 2017.
- Chen, Y., Wang, N., and Zhang, Z. Dark-rank: Accelerating deep metric learning via cross sample similarities transfer, 2018. URL <https://www.aaai.org/ocs/index.php/AAAI/AAAI18/paper/view/17147>.
- Dai, B. and Wipf, D. P. Diagnosing and enhancing VAE models. *CoRR*, abs/1903.05789, 2019. URL <http://arxiv.org/abs/1903.05789>.
- Deng, J., Guo, J., Xue, N., and Zafeiriou, S. Arcface: Additive angular margin loss for deep face recognition. In *2019 IEEE/CVF Conference on Computer Vision and Pattern Recognition (CVPR)*, pp. 4685–4694, 2019. doi: 10.1109/CVPR.2019.00482.
- Duan, Y., Zheng, W., Lin, X., Lu, J., and Zhou, J. Deep adversarial metric learning. In *The IEEE Conference on Computer Vision and Pattern Recognition (CVPR)*, June 2018.
- Furlanello, T., Lipton, Z. C., Tschannen, M., Itti, L., and Anandkumar, A. Born-again neural networks. In Dy, J. G. and Krause, A. (eds.), *Proceedings of the 35th International Conference on Machine Learning, ICML 2018, Stockholmsmässan, Stockholm, Sweden, July 10-15, 2018*, volume 80 of *Proceedings of Machine Learning Research*, pp. 1602–1611. PMLR, 2018. URL <http://proceedings.mlr.press/v80/furlanello18a.html>.
- Ge, W. Deep metric learning with hierarchical triplet loss. In *Proceedings of the European Conference on Computer Vision (ECCV)*, pp. 269–285, 2018.
- Hadsell, R., Chopra, S., and LeCun, Y. Dimensionality reduction by learning an invariant mapping. In *Proceedings of the IEEE Conference on Computer Vision and Pattern Recognition*, 2006.
- Han, J., Zhao, T., and Zhang, C. Deep distillation metric learning. *Proceedings of the ACM Multimedia Asia*, 2019.
- He, K., Zhang, X., Ren, S., and Sun, J. Deep residual learning for image recognition. In *Proceedings of the IEEE*
- He, K., Fan, H., Wu, Y., Xie, S., and Girshick, R. Momentum contrast for unsupervised visual representation learning. In *Proceedings of the IEEE/CVF Conference on Computer Vision and Pattern Recognition (CVPR)*, June 2020.
- Hinton, G., Vinyals, O., and Dean, J. Distilling the knowledge in a neural network. *arXiv preprint arXiv:1503.02531*, 2015.
- Ioffe, S. and Szegedy, C. Batch normalization: Accelerating deep network training by reducing internal covariate shift. pp. 448–456, 2015. URL <http://jmlr.org/proceedings/papers/v37/ioffe15.pdf>.
- Jacob, P., Picard, D., Histace, A., and Klein, E. Metric learning with horde: High-order regularizer for deep embeddings. In *The IEEE Conference on Computer Vision and Pattern Recognition (CVPR)*, 2019.
- Jegou, H., Douze, M., and Schmid, C. Product quantization for nearest neighbor search. *IEEE transactions on pattern analysis and machine intelligence*, 33(1):117–128, 2011.
- Johnson, J., Douze, M., and Jégou, H. Billion-scale similarity search with gpus. *arXiv preprint arXiv:1702.08734*, 2017.
- Kim, S., Kim, D., Cho, M., and Kwak, S. Proxy anchor loss for deep metric learning. In *Proceedings of the IEEE/CVF Conference on Computer Vision and Pattern Recognition (CVPR)*, June 2020.
- Kim, W., Goyal, B., Chawla, K., Lee, J., and Kwon, K. Attention-based ensemble for deep metric learning. In *Proceedings of the European Conference on Computer Vision (ECCV)*, 2018.
- Kingma, D. P. and Ba, J. Adam: A method for stochastic optimization. In Bengio, Y. and LeCun, Y. (eds.), *3rd International Conference on Learning Representations, ICLR 2015, San Diego, CA, USA, May 7-9, 2015, Conference Track Proceedings*, 2015. URL <http://arxiv.org/abs/1412.6980>.
- Krause, J., Stark, M., Deng, J., and Fei-Fei, L. 3d object representations for fine-grained categorization. In *Proceedings of the IEEE International Conference on Computer Vision Workshops*, pp. 554–561, 2013.
- Krogh, A. and Hertz, J. A. A simple weight decay can improve generalization. In *Advances in Neural Information Processing Systems*. 1992.

- Lan, X., Zhu, X., and Gong, S. Self-referenced deep learning. *CoRR*, abs/1811.07598, 2018. URL <http://arxiv.org/abs/1811.07598>.
- Laskar, Z. and Kannala, J. Data-efficient ranking distillation for image retrieval. *CoRR*, abs/2007.05299, 2020. URL <https://arxiv.org/abs/2007.05299>.
- Lin, X., Duan, Y., Dong, Q., Lu, J., and Zhou, J. Deep variational metric learning. In *The European Conference on Computer Vision (ECCV)*, September 2018.
- Liu, B., Rao, Y., Lu, J., Zhou, J., and Hsieh, C. Metadistiller: Network self-boosting via meta-learned top-down distillation. *CoRR*, abs/2008.12094, 2020. URL <https://arxiv.org/abs/2008.12094>.
- Liu, W., Wen, Y., Yu, Z., Li, M., Raj, B., and Song, L. SpheroFace: Deep hypersphere embedding for face recognition. *IEEE Conference on Computer Vision and Pattern Recognition (CVPR)*, 2017.
- Lloyd, S. P. Least squares quantization in pcm. *IEEE Trans. Information Theory*, 28:129–136, 1982.
- Manning, C., Raghavan, P., and Schütze, H. Introduction to information retrieval. *Natural Language Engineering*, 16(1):100–103, 2010.
- Milbich, T., Roth, K., Bharadhwaj, H., Sinha, S., Bengio, Y., Ommer, B., and Cohen, J. P. Diva: Diverse visual feature aggregation for deep metric learning. *CoRR*, abs/2004.13458, 2020. URL <https://arxiv.org/abs/2004.13458>.
- Milbich, T., Roth, K., Brattoli, B., and Ommer, B. Sharing matters for generalization in deep metric learning. *IEEE Transactions on Pattern Analysis and Machine Intelligence*, pp. 1–1, 2020. doi: 10.1109/TPAMI.2020.3009620.
- Misra, I. and van der Maaten, L. Self-supervised learning of pretext-invariant representations. In *2020 IEEE/CVF Conference on Computer Vision and Pattern Recognition, CVPR 2020, Seattle, WA, USA, June 13-19, 2020*, pp. 6706–6716. IEEE, 2020. doi: 10.1109/CVPR42600.2020.00674. URL <https://doi.org/10.1109/CVPR42600.2020.00674>.
- Movshovitz-Attias, Y., Toshev, A., Leung, T. K., Ioffe, S., and Singh, S. No fuss distance metric learning using proxies. In *Proceedings of the IEEE International Conference on Computer Vision*, pp. 360–368, 2017.
- Musgrave, K., Belongie, S. J., and Lim, S. A metric learning reality check. *CoRR*, abs/2003.08505, 2020. URL <https://arxiv.org/abs/2003.08505>.
- Oh Song, H., Xiang, Y., Jegelka, S., and Savarese, S. Deep metric learning via lifted structured feature embedding. In *Proceedings of the IEEE Conference on Computer Vision and Pattern Recognition*, pp. 4004–4012, 2016.
- Opitz, M., Waltner, G., Possegger, H., and Bischof, H. Deep metric learning with bier: Boosting independent embeddings robustly. *IEEE transactions on pattern analysis and machine intelligence*, 2018.
- Park, W., Kim, D., Lu, Y., and Cho, M. Relational knowledge distillation. *2019 IEEE/CVF Conference on Computer Vision and Pattern Recognition (CVPR)*, Jun 2019. doi: 10.1109/cvpr.2019.00409. URL <http://dx.doi.org/10.1109/CVPR.2019.00409>.
- Park, W., Kim, W., You, K., and Cho, M. Diversified mutual learning for deep metric learning. 2020.
- Paszke, A., Gross, S., Chintala, S., Chanan, G., Yang, E., DeVito, Z., Lin, Z., Desmaison, A., Antiga, L., and Lerer, A. Automatic differentiation in pytorch. In *NIPS-W*, 2017.
- Qian, Q., Shang, L., Sun, B., Hu, J., Li, H., and Jin, R. Softtriple loss: Deep metric learning without triplet sampling. In *Proceedings of the IEEE/CVF International Conference on Computer Vision (ICCV)*, October 2019.
- Raghu, A., Raghu, M., Bengio, S., and Vinyals, O. Rapid learning or feature reuse? towards understanding the effectiveness of MAML. In *8th International Conference on Learning Representations, ICLR 2020, Addis Ababa, Ethiopia, April 26-30, 2020*. OpenReview.net, 2020. URL <https://openreview.net/forum?id=rkgMkCEtPB>.
- Rajasegaran, J., Khan, S., Hayat, M., Khan, F. S., and Shah, M. Self-supervised knowledge distillation for few-shot learning. *CoRR*, abs/2006.09785, 2020. URL <https://arxiv.org/abs/2006.09785>.
- Romero, A., Ballas, N., Kahou, S. E., Chassang, A., Gatta, C., and Bengio, Y. Fitnets: Hints for thin deep nets. In Bengio, Y. and LeCun, Y. (eds.), *3rd International Conference on Learning Representations, ICLR 2015, San Diego, CA, USA, May 7-9, 2015, Conference Track Proceedings*, 2015. URL <http://arxiv.org/abs/1412.6550>.
- Roth, K., Brattoli, B., and Ommer, B. Mic: Mining interclass characteristics for improved metric learning. In *Proceedings of the IEEE International Conference on Computer Vision*, pp. 8000–8009, 2019.
- Roth, K., Milbich, T., and Ommer, B. Pads: Policy-adapted sampling for visual similarity learning. In *Proceedings of the IEEE/CVF Conference on Computer Vision and Pattern Recognition (CVPR)*, June 2020a.

- Roth, K., Milbich, T., Sinha, S., Gupta, P., Ommer, B., and Cohen, J. P. Revisiting training strategies and generalization performance in deep metric learning. In III, H. D. and Singh, A. (eds.), *Proceedings of the 37th International Conference on Machine Learning*, volume 119 of *Proceedings of Machine Learning Research*, pp. 8242–8252. PMLR, 13–18 Jul 2020b. URL <http://proceedings.mlr.press/v119/roth20a.html>.
- Sanakoyeu, A., Tschernetzki, V., Buchler, U., and Ommer, B. Divide and conquer the embedding space for metric learning. In *The IEEE Conference on Computer Vision and Pattern Recognition (CVPR)*, 2019.
- Schroff, F., Kalenichenko, D., and Philbin, J. Facenet: A unified embedding for face recognition and clustering. In *Proceedings of the IEEE conference on computer vision and pattern recognition*, pp. 815–823, 2015.
- Sohn, K. Improved deep metric learning with multi-class n-pair loss objective. In *Advances in Neural Information Processing Systems*, pp. 1857–1865, 2016.
- Suárez, J., García, S., and Herrera, F. A tutorial on distance metric learning: Mathematical foundations, algorithms and software. *CoRR*, abs/1812.05944, 2018. URL <http://arxiv.org/abs/1812.05944>.
- Tian, Y., Krishnan, D., and Isola, P. Contrastive representation distillation. *CoRR*, abs/1910.10699, 2019. URL <http://arxiv.org/abs/1910.10699>.
- Tian, Y., Wang, Y., Krishnan, D., Tenenbaum, J. B., and Isola, P. Rethinking few-shot image classification: a good embedding is all you need? *arXiv preprint arXiv:2003.11539*, 2020.
- Wah, C., Branson, S., Welinder, P., Perona, P., and Belongie, S. The caltech-ucsd birds-200-2011 dataset. Technical Report CNS-TR-2011-001, California Institute of Technology, 2011.
- Wang, T. and Isola, P. Understanding contrastive representation learning through alignment and uniformity on the hypersphere. *arXiv preprint arXiv:2005.10242*, 2020.
- Wang, X., Han, X., Huang, W., Dong, D., and Scott, M. R. Multi-similarity loss with general pair weighting for deep metric learning. In *Proceedings of the IEEE/CVF Conference on Computer Vision and Pattern Recognition (CVPR)*, June 2019.
- Wu, C.-Y., Manmatha, R., Smola, A. J., and Krahenbuhl, P. Sampling matters in deep embedding learning. In *Proceedings of the IEEE International Conference on Computer Vision*, pp. 2840–2848, 2017.
- Xuan, H., Souvenir, R., and Pless, R. Deep randomized ensembles for metric learning. In *Proceedings of the European Conference on Computer Vision (ECCV)*, pp. 723–734, 2018.
- Xuan, H., Stylianou, A., and Pless, R. Improved embeddings with easy positive triplet mining. In *Proceedings of the IEEE/CVF Winter Conference on Applications of Computer Vision (WACV)*, March 2020.
- Yu, L., Yazici, V. O., Liu, X., van de Weijer, J., Cheng, Y., and Ramisa, A. Learning metrics from teachers: Compact networks for image embedding. *2019 IEEE/CVF Conference on Computer Vision and Pattern Recognition (CVPR)*, Jun 2019. doi: 10.1109/cvpr.2019.00302. URL <http://dx.doi.org/10.1109/CVPR.2019.00302>.
- Yun, S., Park, J., Lee, K., and Shin, J. Regularizing class-wise predictions via self-knowledge distillation. In *Proceedings of the IEEE/CVF Conference on Computer Vision and Pattern Recognition (CVPR)*, June 2020.
- Zagoruyko, S. and Komodakis, N. Paying more attention to attention: Improving the performance of convolutional neural networks via attention transfer. *CoRR*, abs/1612.03928, 2016. URL <http://arxiv.org/abs/1612.03928>.
- Zhai, A. and Wu, H. Making classification competitive for deep metric learning. *CoRR*, abs/1811.12649, 2018. URL <http://arxiv.org/abs/1811.12649>.
- Zhang, L., Song, J., Gao, A., Chen, J., Bao, C., and Ma, K. Be your own teacher: Improve the performance of convolutional neural networks via self distillation. In *Proceedings of the IEEE/CVF International Conference on Computer Vision (ICCV)*, October 2019a.
- Zhang, L., Song, J., Gao, A., Chen, J., Bao, C., and Ma, K. Be your own teacher: Improve the performance of convolutional neural networks via self distillation. *CoRR*, abs/1905.08094, 2019b. URL <http://arxiv.org/abs/1905.08094>.
- Zhang, Y., Xiang, T., Hospedales, T. M., and Lu, H. Deep mutual learning. In *Proceedings of the IEEE Conference on Computer Vision and Pattern Recognition (CVPR)*, June 2018.
- Zheng, W., Chen, Z., Lu, J., and Zhou, J. Hardness-aware deep metric learning. *The IEEE Conference on Computer Vision and Pattern Recognition (CVPR)*, 2019.

Supplementary: Simultaneous Similarity-based Self-Distillation for Deep Metric Learning

A. More Benchmark & Implementation Details

In this part, we report all relevant benchmark details omitted in the main document as well as further implementation details.

A.1. Benchmarks

CUB200-2011 (Wah et al., 2011) contains 200 bird classes over 11,788 images, where the first and last 100 classes with 5864/5924 images are used for training and testing, respectively.

CARS196 (Krause et al., 2013) contains 196 car classes and 16,185 images, where again the first and last 98 classes with 8054/8131 images are used to create the training/testing split.

Stanford Online Products (SOP) (Oh Song et al., 2016) is build around 22,634 product classes over 120,053 images and contains a provided split: 11318 selected classes with 59551 images are used for training, and 11316 classes with 60502 images for testing.

A.2. Implementation

We now provide further details regarding the training and testing setup utilized. For any study except the comparison against the state-of-the-art (Table 2) which uses different backbones and embedding dimensions, we follow the setup used by (Roth et al., 2020b)¹: This includes a ResNet50 (He et al., 2016) with frozen Batch-Normalization (Ioffe & Szegedy, 2015), normalization of the output embeddings with dimensionality 128 and optimization with Adam (Kingma & Ba, 2015) using a learning rate of 10^{-5} and weight decay of $3 \cdot 10^{-4}$. The input images are randomly resized and cropped from the original image size to 224×224 for training. Further augmentation by random horizontal flipping with $p = 0.5$ is applied. During testing, center crops of size 224×224 are used. The batchsize is set to 112.

Training runs on CUB200-2011 and CARS196 are done over 150 epochs and 100 epochs for SOP for all experiments without any learning rate scheduling, except for the state-of-the-art experiments (see again 2). For the latter, we made use of slightly longer training to account for conservative learning rate scheduling, which is similarly done across reference methods noted in tab. 2. Schedule and decay values are determined over validation subset performances. All baseline DML objectives we apply our self-distillation module *S2SD* on use the default parameters noted in (Roth et al., 2020b) with the single exception of Margin Loss on SOP, where we found class margins $\beta = 0.9$ to be more beneficial for distillation than the default $\beta = 1.2$. This was done as changing from $\beta = 1.2$ to $\beta = 0.9$ had no notable impact on the baseline performance. Finally, similar to (Kim et al., 2020), we found a warmup epoch of all MLPs to improve convergence on SOP. Spectral decay computations in §5.3 follow the setting described in Supp. D.

We implement everything in PyTorch (Paszke et al., 2017). Experiments are done on GPU servers containing Nvidia Titan X, P100 and T4s, however memory usage never exceeds 12GB. Each result is averaged over five seeds, and for the sake of reproducibility and result validity, we report mean and standard deviation, even though this is commonly neglected in DML literature.

¹Repository: github.com/Confusezius/Revisiting_Deep_Metric_Learning_PyTorch

B. Baseline Methods

This section provides a more detailed explanation of the DML baseline objectives we used alongside our self-distillation module *S2SD* in the experimental section 4. For additional details, we refer to the supplementary material in (Roth et al., 2020b). For the mathematical notation, we refer to Section 3.1. We use $\psi = f \circ \phi$ to denote the feature network ϕ with embedding f , and ψ_i the embedding of a sample x_i . Finally, alongside the method descriptions we provide the used hyperparameters.

Margin Loss (Wu et al., 2017) builds on triplet/pair-based losses, but introduces both class-specific, learnable boundaries $\{\beta_{y_k}\}_{k=1\dots C}$ (with number of classes C) between positive and negative pairs, as well as distance-based sampling for negatives:

$$\mathcal{L}_{\text{margin}} = \sum_{x_i, x_j \in \mathcal{P}_{\mathcal{B}}} [m + (-1)^{\mathbb{1}_{y_i=y_j}} (\beta_{y_i} - d(\psi_i, \psi_j))]_+ \quad (9)$$

$$p(x_j | x_i, y_i \neq y_j) = \min \left(\lambda, \left[d(\psi_i, \psi_j)^{n-2} \left(1 - \frac{1}{4} d(\psi_i, \psi_j)^2 \right)^{\frac{n-3}{2}} \right]^{-1} \right) \quad (10)$$

where $\mathcal{P}_{\mathcal{B}}$ denotes the available pairs in minibatch \mathcal{B} , and n the embedding dimension. Throughout this work, we use $\beta = 1.2$ except for *S2SD* on SOP, where we found $\beta = 0.9$ to work better without changing the baseline performance. We set the learning rate for the class boundaries as $5 \cdot 10^{-4}$, and margin $m = 0.2$.

Regularized Margin Loss (Roth et al., 2020b) proposes a simple regularization scheme on the margin loss that increases the number of directions of significant variance in the embedding space by randomly exchanging a negative sample with a positive one with probability p_{switch} . For ResNet-backbones, we use $p_{\text{switch}} = 0.4$ for CUB200, $p_{\text{switch}} = 0.35$ for CARS196 and $p_{\text{switch}} = 0.15$ for SOP as done in (Roth et al., 2020b). For Inception-based backbones, we set $p_{\text{switch}} = 0.15$ for CUB200 and CARS196 and $p_{\text{switch}} = 0.3$ for SOP.

Multisimilarity Loss (Wang et al., 2019) incorporates more similarities into training by operating directly on all positive and negative samples for an anchor x_i , while also incorporating a sampling operation that encourages the usage of harder training samples:

$$d_c^*(i, j) = \begin{cases} d_c(\psi_i, \psi_j) & d_c(\psi_i, \psi_j) > \min_{j \in \mathcal{P}_i} d_c(\psi_i, \psi_j) - \epsilon \\ d_c(\psi_i, \psi_j) & d_c(\psi_i, \psi_j) < \max_{k \in \mathcal{N}_i} d_c(\psi_i, \psi_k) + \epsilon \\ 0 & \text{otherwise} \end{cases} \quad (11)$$

$$\begin{aligned} \mathcal{L}_{\text{multisim}} = & \frac{1}{b} \sum_{i \in \mathcal{B}} \left[\frac{1}{\alpha} \log \left[1 + \sum_{j \in \mathcal{P}_i} \exp(-\alpha(d_c^*(\psi_i, \psi_j) - \lambda)) \right] \right] \\ & + \sum_{i \in \mathcal{B}} \left[\frac{1}{\beta} \log \left[1 + \sum_{k \in \mathcal{N}_i} \exp(\beta(d_c^*(\psi_i, \psi_k) - \lambda)) \right] \right] \end{aligned} \quad (12)$$

where d_c denotes the cosine similarity instead of the euclidean distance, and $\mathcal{P}_i/\mathcal{N}_i$ the set of positives and negatives for x_i in the minibatch, respectively. We use the default values $\alpha = 2$, $\beta = 40$, $\lambda = 0.5$ and $\epsilon = 0.1$.

C. Evaluation Metrics

The evaluation metrics used throughout this work are recall @ 1 (R@1), recall @ 2 (R@2) and Normalized Mutual Information (NMI), capturing two distinct embedding space properties.

Recall@K, see e.g. in (Jegou et al., 2011), especially Recall@1 and Recall@2, is the primary metric used to compare the performance of DML methods and approaches, as it offers strong insights into retrieval performances of the learned embedding spaces. Given the set of embedded samples $\psi_i \in \Psi$ with $\psi_i = \psi(x_i)$ and $x_i \in \mathcal{X}$, and the sorted set of k nearest neighbours for any sample ϕ_a ,

$$\mathcal{F}_a^k = \min_{d(\phi_a, \cdot)} \text{sort} \arg \min_{\mathcal{F} \subset \mathcal{X}, |\mathcal{F}|=k} \sum_{x_f \in \mathcal{F}} d(\phi_a, \phi_f) \quad (13)$$

Recall@K is measured as

$$\text{Recall@K} = \frac{1}{|\mathcal{X}|} \sum_{x_i \in \mathcal{X}} \begin{cases} 1 & \exists x_k \in \mathcal{F}_i^k \text{ s.t. } y_k = y_i \\ 0 & \text{otherwise} \end{cases} \quad (14)$$

which evaluates how likely semantically corresponding pairs (as determined here by the labelling $y_i \in \mathcal{Y}$) will occur in a neighbourhood of size k .

Normalized Mutual Information (NMI), see (Manning et al., 2010), evaluates the clustering quality of the embedded samples Ψ (taken from \mathcal{X}). It is computed by first clustering with K cluster centers, usually corresponding to the number of classes available, using a cluster method of choice s.a. K-Means (Lloyd, 1982). This assigns each sample x_i a cluster label/id ω_i based on the nearest cluster centroid. With $\eta_k = \{i | \omega_i = \omega_k\}$ the set of samples with cluster label, $\Omega = \{\eta_k\}_k^K$ the set of cluster sets, $\nu_k = \{i | y_i = y_k\}$ the set of samples with true label y_k and $\Upsilon = \{\nu_k\}_k^K$ the set of class label sets, the Normalized Mutual Information is given as

$$\text{NMI}(\Omega, \Upsilon) = \frac{I(\Omega, \Upsilon)}{2 \cdot (H(\Omega) + H(\Upsilon))} \quad (15)$$

with mutual information $I(\cdot, \cdot)$ and entropy $H(\cdot)$.

D. Generalization Metrics

Embedding Space Density. Given sets of embeddings Ψ , we first define the average inter-class distance as

$$\pi_{\text{inter}}(\Psi) = \frac{1}{Z_{\text{inter}}} \sum_{y_l, y_k, l \neq k} d(\mu(\Psi_{y_l}), \mu(\Psi_{y_k})) \quad (16)$$

which measures the average distances between groups of embeddings with respective classes y_l and y_k , estimated by the respective class centers $\mu(\cdot)$. Z_{inter} denotes a normalization constant based on the number of available classes. We also introduce the average intra-class distance as the mean distance between samples within their respective class

$$\pi_{\text{intra}}(\Psi) = \frac{1}{Z_{\text{intra}}} \sum_{y_l \in \mathcal{Y}} \sum_{\psi_i, \psi_j \in \Psi_{y_l}, i \neq j} d(\psi_i, \psi_j) \quad (17)$$

again with normalization constant Z_{intra} and set of embeddings with class y_l , Ψ_{y_l} . Given these two quantities, the embedding space density is then defined as

$$\pi_{\text{ratio}}(\Psi) = \frac{\pi_{\text{intra}}(\Psi)}{\pi_{\text{inter}}(\Psi)} \quad (18)$$

and effectively measured how densely samples and classes are grouped together. (Roth et al., 2020b) show that optimizing the DML problem while keeping the embedding space density high, i.e. without aggressive clustering, encourages better generalization to unseen test classes.

Spectral Decay. The spectral decay metric $\rho(\Psi)$ defines the KL-divergence between the (sorted) spectrum of D singular values $\mathcal{S}_{\Psi}^{\text{singular}}$ (obtained via Singular Value Decomposition (SVD)) and a D -dimensional uniform distribution \mathcal{U}_D , and is inversely related to the entropy of the embedding space:

$$\rho(\Psi) = \mathcal{D}_{\text{KL}}(\mathcal{U}_D, \mathcal{S}_{\Psi}^{\text{singular}}) \quad (19)$$

It does not account for class distributions. (Roth et al., 2020b) show that doing DML while encouraging a high-entropy feature space notably benefits the generalization performance. In our experiments, we disregard the first 10 singular vectors (out of 128) to highlight the feature diversity. This is important, as we evaluate the spectral decay within the same objectives, which results in the first few singular values to be highly similar.

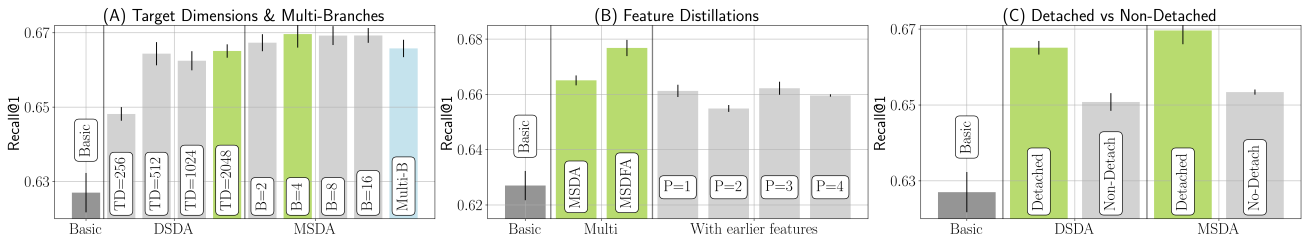


Figure 4. *Additional ablations.* (A) Increasing target dimensions offers notable improvements. We opt for a target dimension of 2048 due to slightly higher mean improvements. For multiple embedding branches ($\#B$), there seems to be an optimum at four branches. (B) Furthermore, feature distillation gives another notable boost. However, this only holds for the globally averaged penultimate feature representation. When distilling more fine-grained feature representations, performance degenerates (where $\#P$ denotes smaller pooling windows applied to the penultimate feature representation). (C) We show that detached auxiliary branches for distillation are crucial to higher improvements, as we want the reference embedding space to approximate the higher-dimensional one.

E. Additional Experiments

This part extends the set of ablation experiments performed in section 5.4 in the main paper.

a. Detaching target spaces for distillation. We examine whether it is preferable to detach the target embeddings from the distillation loss (see eq. 3), as we want the reference embedding space to approximate the higher-dimensional relations. Similarly, we do not want the target embedding networks g_i to reduce high-dimensional to lower-dimensional relations to optimizer for the distillation constraint. As can be seen in fig 4C, it is indeed the case that detaching the target embedding spaces is notably beneficial for a stronger reference embedding, supporting the previous motivation.

b. Influence of varying target dimensions. As noted at the beginning of section 4, we set the target dimension for dual self-distillation (DSD) to $d = 2048$, which we motivate through a small ablation study in fig. 4A, with TD denoting the target dimension of choice. As can be seen, benefits plateau when the target dimension reaches more than four times the reference dimension. However, to be directly comparable to high-dimensional reference settings, we set $d = 2048$ as default.

c. Ablating multiple distillation scales. Going further, we extend the module with additional embedding branches to the multiscale self-distillation approach (MSD), all operating in different, but higher-than-reference dimension. As already shown in Figure 3B in the main paper, there is a benefit of multiscale distillations by encouraging reusable sample relations. In this part, we motivate the choice of four target branches (as noted in sec. 4). Looking at figure 4A, where B denotes the number of additional target spaces, we can see a benefit in multiple additional target spaces of ascending dimension. As the improvements saturate after $B = 4$, we simply set this as the default value. However, the additional benefits of going to multiscale from dual distillation are not as high as going from no to dual target space distillation, showcasing the general benefit of high-dimensional concurrent self-distillation. Finally, we highlight that a multiscale approach slightly outperforms a multibranch distillation setup (Fig. 4A, *Multi-B*) where each target branch has the same target dimension of 2048 while introducing less additional parameters.

d. Finer-grained feature distillation. As already shown in section 4 and again in figure 4B, we see benefits of feature distillation, using the (globally averaged) normalized penultimate feature space. It therefore makes sense to investigate the benefits of distilling even more fine-grained feature representation. Defining $\mathcal{P} = [(3, 3), (1, 1), (2, 2), (4, 1)]$ as the pooling window size applied to the non-average penultimate feature representation, we investigate less compressed feature representation space. As can be seen in fig. 4B, where P denotes the index to \mathcal{P} , there appears to be no benefits in distilling feature representations higher up the network.

e. Runtime comparison of base dimensionalities. We highlight relative retrieval times at different base dimensionalities in Tab. 3 using `faiss` (Johnson et al., 2017) on a NVIDIA 1080Ti and a synthetic set of $N = 250000$ embeddings of dimensionality $d \in [32, 64, 128, 256, 512, 1024, 2048]$. With *S2SD* matching $d = 64/128$ to base dimensionalities $d = 512/2048$ (see §5.3), runtime can be reduced by up to a magnitude.

Dimensionality d	32	64	128	256	512	1024	2048
Runtime (s)	1.54±0.00	1.98±0.00	2.71±0.00	4.35±0.00	7.38±0.01	13.83±0.02	27.21±0.17

Table 3. Sample retrieval times for 250000 embeddings with varying base dimensionalities.

F. Pseudo-Code

```

1 import torch, torch.nn as nn, torch.nn.functional as F
2 from F import normalize as norm
3
4 """
5 Parameters:
6     self.base_criterion: base DML objective
7     self.trgt_criteria: list of DML objectives for target spaces
8     self.trgt_nets: Module list of auxiliary embedding MLPs
9     self.dist_gamma: distillation weight
10    self.it_before_feat_distill: iterations before feature distill
11 """
12
13 def forward(self, batch, labels, pre_batch, **kwargs):
14     """
15     Args:
16         batch: image embeddings, shape: bs x d
17         labels: image labels, shape: bs
18         pre_batch: penultimate network features, shape: bs x d*
19     """
20     bs, batch = len(batch), norm(batch, dim=-1)
21
22     ### Compute ref. sample relations and loss on ref. embedding space
23     base_smat = batch.mm(batch.T)
24     base_loss = self.base_criterion(batch, labels, **kwargs)
25
26     ### Do global average pooling (and max. pool if wanted)
27     avg_pre_batch = nn.AdaptiveAvgPool2d(1)(pre_batch).view(bs,-1)
28     avg_pre_batch += nn.AdaptiveMaxPool2d(1)(pre_batch).view(bs,-1)
29
30     ### Computing MSDA loss (Targets & Distillations)
31     dist_losses, trgt_losses = [], []
32     for trgt_crit, trgt_net in zip(self.trgt_criteria, self.trgt_nets):
33         trgt_batch = norm(trgt_net(avg_pre_batch), dim=-1)
34         trgt_loss = trgt_crit(trgt_batch, labels, **kwargs)
35         trgt_smat = trgt_batch.mm(trgt_batch.T)
36         base_trgt_dist = self.kl_div(base_smat, trgt_smat.detach())
37         trgt_losses.append(trgt_loss)
38         dist_losses.append(base_trgt_dist)
39
40     ### MSDA loss
41     multi_dist_loss = (base_loss + torch.stack(trgt_losses).mean()) / 2.
42     multi_dist_loss += self.dist_gamma * torch.stack(dist_losses).mean()
43
44     ### Distillation of penultimate features -> MSDFA
45     src_feat_dist = 0
46     if self.it_count >= self.it_before_feat_distill:
47         n_avg_pre_batch = norm(avg_pre_batch, dim=-1).detach()
48         avg_feat_smat = n_avg_pre_batch.mm(n_avg_pre_batch.T)
49         src_feat_dist = self.kl_div(base_smat, avg_feat_smat.detach())
50
51     ### Total S2SD training objective
52     total_loss = multi_distill_loss + self.dist_gamma * src_feat_dist
53     self.it_count += 1
54     return total_loss
55
56 def kl_div(self, A, B, T=1):
57     log_p_A = F.log_softmax(A/self.T, dim=-1)
58     p_B = F.softmax(B/self.T, dim=-1)
59     kl_d = F.kl_div(log_p_A, p_B, reduction='sum') * T * 2 / A.size(0)
60     return kl_d
    
```

Listing 1. PyTorch Implementation for S2SD.

G. Detailed Evaluation Results

This table contains all method ablations for a fair evaluation as used in Section 5.2 and Table 1.

Table 4. Detailed Comparison of Recall@1 and NMI performances against well performing DML objectives examined in section 5.2. This is the complete version to table 1. All results are computed over 5-run averages. (*) For Margin Loss and SOP, we found $\beta = 0.9$ to give better distillation results without notably influencing baseline performance.

Benchmarks→	CUB200-2011		CARS196		SOP	
Approaches ↓	R@1	NMI	R@1	NMI	R@1	NMI
Margin(*)	63.09 ± 0.46	68.21 ± 0.33	79.86 ± 0.33	67.36 ± 0.34	78.43 ± 0.07	90.40 ± 0.03
+ DSD	65.11 ± 0.18	69.65 ± 0.44	83.19 ± 0.18	69.28 ± 0.56	79.05 ± 0.12	90.52 ± 0.18
+ DSDA	65.77 ± 0.55	69.85 ± 0.25	83.92 ± 0.08	69.95 ± 0.21	77.78 ± 0.15	90.29 ± 0.08
+ MSD	66.13 ± 0.34	70.83 ± 0.27	83.63 ± 0.31	69.80 ± 0.36	79.26 ± 0.15	90.60 ± 0.10
+ MSDA	66.14 ± 0.32	70.82 ± 0.18	84.31 ± 0.12	70.17 ± 0.30	78.04 ± 0.11	90.45 ± 0.05
+ MSDF	67.58 ± 0.32	71.47 ± 0.19	85.55 ± 0.23	71.68 ± 0.54	79.63 ± 0.14	90.70 ± 0.09
+ MSDFFA	67.21 ± 0.23	71.43 ± 0.25	86.45 ± 0.35	71.46 ± 0.24	78.82 ± 0.09	90.49 ± 0.06
R-Margin	64.93 ± 0.42	68.36 ± 0.32	82.37 ± 0.13	68.66 ± 0.47	77.58 ± 0.11	90.42 ± 0.03
+ DSD	66.58 ± 0.08	70.03 ± 0.41	84.64 ± 0.16	70.87 ± 0.18	77.86 ± 0.10	90.50 ± 0.03
+ DSDA	67.11 ± 0.43	70.39 ± 0.48	84.32 ± 0.36	70.85 ± 0.16	77.79 ± 0.11	90.37 ± 0.04
+ MSD	66.81 ± 0.27	70.47 ± 0.16	85.01 ± 0.10	71.67 ± 0.40	78.00 ± 0.06	90.47 ± 0.04
+ MSDA	67.31 ± 0.41	71.01 ± 0.24	85.34 ± 0.17	71.85 ± 0.20	77.93 ± 0.06	90.29 ± 0.08
+ MSDF	68.12 ± 0.30	71.80 ± 0.33	85.78 ± 0.22	72.24 ± 0.31	78.57 ± 0.09	90.58 ± 0.02
+ MSDFFA	68.58 ± 0.26	71.64 ± 0.40	86.81 ± 0.35	71.48 ± 0.29	78.00 ± 0.11	90.41 ± 0.02
Multisimilarity	62.80 ± 0.70	68.55 ± 0.38	81.68 ± 0.19	69.43 ± 0.38	77.99 ± 0.09	90.00 ± 0.02
+ DSD	65.57 ± 0.26	70.08 ± 0.33	83.51 ± 0.20	70.30 ± 0.05	78.23 ± 0.04	90.08 ± 0.04
+ DSDA	66.60 ± 0.43	70.74 ± 0.40	84.42 ± 0.28	70.36 ± 0.34	77.92 ± 0.12	89.99 ± 0.04
+ MSD	65.80 ± 0.16	70.53 ± 0.01	83.98 ± 0.10	71.34 ± 0.09	78.42 ± 0.09	90.09 ± 0.03
+ MSDA	66.96 ± 0.36	70.77 ± 0.05	85.04 ± 0.14	71.09 ± 0.23	77.98 ± 0.05	90.02 ± 0.04
+ MSDF	67.04 ± 0.29	71.87 ± 0.19	85.69 ± 0.19	72.77 ± 0.13	78.59 ± 0.08	90.09 ± 0.06
+ MSDFFA	67.68 ± 0.29	71.40 ± 0.21	85.89 ± 0.15	71.45 ± 0.26	78.07 ± 0.06	89.88 ± 0.10

H. Evaluation Results using mAP@R

This table measures performance of methods investigated in Table 1 using the mAP@R(@1000) metric used in (Roth et al., 2020b). The results here coincide with those measured using Recall@1. This comes at no surprise, as both metrics are strongly correlated when measuring the performance of Deep Metric Learning methods (Roth et al., 2020b).

I. Detailed Ablation Results

Detailed values to the ablation experiments done in section 5.4 and E.

Table 5. Detailed Comparison of $mAP@R$ (as used in (Roth et al., 2020b) and (Musgrave et al., 2020) and based on the formulation used in (Roth et al., 2020b)) against well performing DML objectives examined in section 5.2.. All results are computed over 5-run averages. (*) For Margin Loss and SOP, we found $\beta = 0.9$ to give better distillation results without notably influencing baseline performance. **Bold** denotes best results per objective and dataset. **Bluebold** denotes best performance per dataset.

Benchmarks→	CUB200-2011	CARS196	SOP
Approaches ↓	mAP	mAP	mAP
Margin(*)	32.63 ± 0.40	32.50 ± 0.28	46.90 ± 0.16
+ DSD	33.85 ± 0.38	34.01 ± 0.39	47.39 ± 0.18
+ MSD	34.79 ± 0.35	34.64 ± 0.31	48.17 ± 0.07
+ MSDF	35.68 ± 0.29	35.26 ± 0.41	48.24 ± 0.10
+ MSDFA	35.98 ± 0.23	35.98 ± 0.40	47.04 ± 0.26
R-Margin	33.38 ± 0.27	34.57 ± 0.30	46.02 ± 0.14
+ DSD	34.46 ± 0.30	35.12 ± 0.22	46.20 ± 0.19
+ MSD	35.11 ± 0.41	35.78 ± 0.40	46.59 ± 0.16
+ MSDF	35.99 ± 0.36	37.32 ± 0.40	47.08 ± 0.17
+ MSDFA	36.25 ± 0.37	37.67 ± 0.35	46.71 ± 0.16
Multisimilarity	30.92 ± 0.49	31.92 ± 0.44	46.23 ± 0.08
+ DSD	33.20 ± 0.34	33.67 ± 0.27	46.21 ± 0.15
+ MSD	34.00 ± 0.35	34.67 ± 0.26	46.45 ± 0.11
+ MSDF	35.16 ± 0.32	35.52 ± 0.51	46.52 ± 0.17
+ MSDFA	35.35 ± 0.24	35.13 ± 0.35	45.39 ± 0.28

Table 6. Additional ProxyAnchor (Kim et al., 2020) results with and without $S2SD$ variants using the proposed, but different, default architecture in (Kim et al., 2020) to highlight that $S2SD$ works equally well on already strong proxy-based objectives objectives with different architectural settings as well.

Benchmarks→	CUB200-2011		CARS196		SOP	
Setting	R@1	NMI	R@1	NMI	R@1	NMI
ProxyAnchor	64.58 ± 0.23	68.95 ± 0.24	82.55 ± 0.41	69.49 ± 0.30	78.33 ± 0.08	90.24 ± 0.06
+ DSD	65.50 ± 0.47	69.97 ± 0.55	83.52 ± 0.11	70.76 ± 0.17	78.33 ± 0.08	90.24 ± 0.06
+ MSD	65.92 ± 0.28	69.88 ± 0.21	83.99 ± 0.33	70.95 ± 0.19	78.47 ± 0.03	90.29 ± 0.06
+ MSDF	66.71 ± 0.12	70.60 ± 0.24	85.20 ± 0.09	71.19 ± 0.18	78.50 ± 0.04	90.31 ± 0.03

Table 7. Experiment: Comparison of concurrent self-distillation against standard 2-stage distillation. This table also shows that training without distillation (*Joint*) or training in high dimension while learning a detached low-dimensional embedding layer (*Concur.*) does not benefit performance notably. See fig. 3A. All results are computed over 5-run averages.

Experiment	Setting	R@1
Distillation	Best Teacher (d=1024)	66.04 ± 0.17
	Base Student (d=128)	62.70 ± 0.53
	Distill Student (d=128)	63.89 ± 0.14
	Concur. Student (d=128)	63.08 ± 0.42
	Joint Student (d=128)	62.93 ± 0.22
	DSD (d=128)	65.57 ± 0.26
	DSDA (d=128)	66.51 ± 0.18
	MSDA (d=128)	66.96 ± 0.36
	MSDFA (d=128)	67.68 ± 0.29

Table 8. Experiment: Benefit of self-distillation across embedding dimensionalities. These results go along with 3B. All results are computed over 5-run averages.

Experiment	Setting	R@1	Setting	R@1
Embedding Dimensionality	Base (d=16)	48.18 ± 0.54	MSD (d=256)	66.90 ± 0.11
	Basic (d=32)	54.54 ± 0.42	MSD (d=512)	67.07 ± 0.02
	Basic (d=64)	59.31 ± 0.26	MSD (d=1024)	66.69 ± 0.11
	Basic (d=128)	62.70 ± 0.53	MSD (d=2048)	66.68 ± 0.18
	Basic (d=256)	64.39 ± 0.30	MSDA (d=16)	51.57 ± 0.39
	Basic (d=512)	65.95 ± 0.19	MSDA (d=32)	61.55 ± 0.23
	Basic (d=1024)	66.04 ± 0.17	MSDA (d=64)	64.94 ± 0.50
	Basic (d=2048)	66.03 ± 0.20	MSDA (d=128)	66.96 ± 0.36
	DSD (d=16)	49.92 ± 0.09	MSDA (d=256)	67.63 ± 0.34
	DSD (d=32)	59.75 ± 0.78	MSDA (d=512)	67.76 ± 0.26
	DSD (d=64)	62.75 ± 0.15	MSDA (d=1024)	67.79 ± 0.10
	DSD (d=128)	65.57 ± 0.26	MSDA (d=2048)	67.33 ± 0.09
	DSD (d=256)	66.34 ± 0.07	MSDF (d=16)	51.99 ± 0.57
	DSD (d=512)	66.89 ± 0.15	MSDF (d=32)	61.61 ± 0.41
	DSD (d=1024)	66.57 ± 0.11	MSDF (d=64)	65.31 ± 0.23
	DSD (d=2048)	66.54 ± 0.28	MSDF (d=128)	66.66 ± 0.29
	DSDA (d=16)	50.77 ± 0.71	MSDF (d=256)	67.47 ± 0.11
	DSDA (d=32)	60.13 ± 0.45	MSDF (d=512)	67.59 ± 0.03
	DSDA (d=64)	63.84 ± 0.36	MSDF (d=1024)	67.40 ± 0.15
	DSDA (d=128)	66.51 ± 0.18	MSDF (d=2048)	67.01 ± 0.35
	DSDA (d=256)	67.13 ± 0.24	MSDFA (d=16)	52.96 ± 0.44
	DSDA (d=512)	67.54 ± 0.24	MSDFA (d=32)	61.98 ± 0.36
	DSDA (d=1024)	67.27 ± 0.22	MSDFA (d=64)	65.19 ± 0.40
	DSDA (d=2048)	67.33 ± 0.30	MSDFA (d=128)	67.68 ± 0.29
MSD (d=16)	50.51 ± 0.21	MSDFA (d=256)	68.48 ± 0.28	
MSD (d=32)	60.00 ± 0.28	MSDFA (d=512)	69.06 ± 0.14	
MSD (d=64)	63.74 ± 0.24	MSDFA (d=1024)	69.08 ± 0.22	
MSD (d=128)	65.80 ± 0.16	MSDFA (d=2048)	69.29 ± 0.35	

Table 9. Experiment: Methods of distillation between reference and target embedding spaces. See fig. 3C. Used Method: **DSDA**. All results are computed over 5-run averages.

Experiment	Setting	R@1
Distillation Methods	R-KL	66.51 ± 0.18
	Cos	65.73 ± 0.27
	Eucl	65.61 ± 0.28
	KL-Full	65.91 ± 0.32
	KL-Mean	64.00 ± 0.55
	Basic	62.70 ± 0.53

Table 10. Experiment: Structure of the secondary branch. More specifically, this table contains specific values used in fig. 3D. Used Method: **DSDA**. All results are computed over 5-run averages.

Experiment	Setting	R@1
Secondary Branch Structure	2 Layers	66.51 ± 0.18
	3 Layers	66.03 ± 0.29
	4 Layers	65.76 ± 0.65
	Linear	65.28 ± 0.48
	Basic	62.70 ± 0.53

Table 11. Experiment: Different distillation hierarchies. See fig. 3E. Used Method: **MSDA**. All results are computed over 5-run averages.

Experiment	Setting	R@1
Distillation Hierarchies	Basic	62.70 ± 0.53
	Straight	66.96 ± 0.36
	Fully	65.58 ± 0.46
	Stacked	65.21 ± 0.25

Table 12. Experiment: Influence of distillation weight γ . See fig. 3F. Used Method: **DSD**. All results are computed over 5-run averages.

Experiment	Setting	R@1 CUB200	R@1 CARS196	R@1 SOP
Weight Ablation	0.0	62.70 \pm 0.53	81.32 \pm 0.36	77.78 \pm 0.06
	0.2	62.85 \pm 0.41	81.65 \pm 0.40	78.22 \pm 0.07
	1.0	62.92 \pm 0.16	81.92 \pm 0.51	78.71 \pm 0.10
	5.0	63.88 \pm 0.19	82.96 \pm 0.10	79.05 \pm 0.12
	20.0	65.43 \pm 0.21	83.50 \pm 0.35	78.72 \pm 0.10
	50.0	65.57 \pm 0.26	83.51 \pm 0.33	78.10 \pm 0.13
	250.0	65.04 \pm 0.33	82.25 \pm 0.62	77.41 \pm 0.12
	1000.0	63.32 \pm 0.36	77.00 \pm 0.66	77.01 \pm 0.08
	2000.0	62.76 \pm 0.31	72.72 \pm 0.85	76.37 \pm 0.11
	5000.0	62.05 \pm 0.62	70.90 \pm 0.97	75.42 \pm 0.20

Table 13. Experiment: Evaluation target dimensions and levels of multiscale distillation. See fig. 4A. All results are computed over 5-run averages.

Experiment	Setting	R@1
Target Dimensionalities	Basic	62.70 \pm 0.53
	DSDA, TD=256	64.82 \pm 0.18
	DSDA, TD=512	66.44 \pm 0.31
	DSDA, TD=1024	66.25 \pm 0.26
	DSDA, TD=2048	66.51 \pm 0.18
MultiScale distillation	MSDA, #B=2	66.76 \pm 0.23
	MSDA, #B=4	66.96 \pm 0.36
	MSDA, #B=8	66.72 \pm 0.25
	MSDA, #B=16	66.59 \pm 0.20

Table 14. Experiment: Is it beneficial to distill more fine-grained features? See fig. 4B. All results are computed over 5-run averages.

Experiment	Setting	R@1
Earlier Features	Basic	62.70 \pm 0.53
	MSDA	66.96 \pm 0.36
	MSDFA	67.68 \pm 0.29
	MSDFA, #P=1	66.13 \pm 0.22
	MSDFA, #P=2	65.49 \pm 0.12
	MSDFA, #P=3	66.22 \pm 0.24
	MSDFA, #P=4	65.96 \pm 0.04

Table 15. Experiment: Is it necessary to detach auxiliary branches for distillation? See fig. 4C. All results are computed over 5-run averages.

Experiment	Setting	R@1
Branch Detaching	Basic	62.70 \pm 0.53
	DSDA, Detached	66.51 \pm 0.18
	DSDA, Non-Detach	65.08 \pm 0.23
	MSDA, Detached	66.96 \pm 0.36
	MSDA, No-Detach	65.34 \pm 0.07